eprints@whiterose.ac.uk
https://eprints.whiterose.ac.uk/

Performance and Flow Characteristics of Miniature EHD Air Blowers for Thermal Management Applications

Abdulmajeed A. Ramadhan[a,b,*], N. Kapur[a], J.L. Summers[a,c], H.M. Thompson[a]

[a] School of Mechanical Engineering, University of Leeds, UK.
[b] Department of Mechanical Engineering, University of Anbar, Iraq.
[c] Research Institutes of Sweden, Swedish Institute of Computer Science North, Lulea, Sweden.

Abstract

Electrohydrodynamic (EHD) air blowers are receiving increasing attention as a thermal management cooling solution to overcome the restrictions of traditional rotary cooling systems used in small-scale consumer electronics. In this work, the performance and flow pattern characteristics of miniature EHD air blowers are evaluated for practical convective heat transfer applications, based on device size, operating voltage and power, and generated flow rate. For a range of blower heights up to 10 mm, two-dimensional (2D) and three-dimensional (3D) numerical models of a wire-to-plane EHD channel configuration are developed and validated against previous experimental data. Investigation of the influence of blower sidewalls, based on width parameter, on flow characteristics reveals that the 2D simulations for short and wide blower domains are valid to predict the generated flow rates effectively compared to that obtained by the means of 3D simulations. An optimized combined EHD blower is developed as a flow-controlled cooling system in thermal management applications, which minimizes the required operating voltages for specified flow rates. Comparisons against commercial rotary blowers demonstrate that the miniature EHD blowers are more competitive as cooling solutions for compact applications and extended heated surfaces based on transduction efficiency, blower size, flow production of uniform velocity profile, and power consumption.

* Corresponding author.
School of Mechanical Engineering, University of Leeds, UK.
E-mail addresses: mnaarr@leeds.ac.uk , aar7sh@gmail.com (A.A. Ramadhan).

1. Introduction

Due to the inexorable increase in heat generation from microelectronic devices and components, the development of effective thermal management cooling solutions has become an increasingly critical challenge for the academic community, engineering designers and the electronics industry. Forced-air convection induced by rotary fans remains the most popular cooling method for most electronic devices especially in portable and consumer products due to convenience, design flexibility and low manufacturing

costs as well as the capability to dissipate the generated heat to the ambient environment, which is ultimately a required feature for most air-cooled devices. However, the increasing performance of microelectronics has led not only to a higher heat generation in electronic components but to smaller-scale devices. Associated with this trend are the considerable challenges of miniaturizing rotary fans to meet the required heat dissipation in thin applications, where the device thickness is a critical and limiting factor [1].

Typically, the fan blade profile height and motor design are the main key factors that determine the fan performance, which can be predicted using well-known fan scaling laws. In their experimental study, Walsh et al. [2] showed that the magnitudes of flow rate, pressure rise, and power consumption calculated by scaling laws for miniaturized centrifugal fans, which are usually used in thin electronic devices, are inaccurate compared to those of experiments. Their results revealed that it is not valid to apply fan scaling laws based on only blade profile height to determine fan performance independently of fan diameter. Based on fan aspect ratio, which is defined as the ratio of the fan blade height to its diameter, their results revealed that the maximum flow rate lies in a range of aspect ratio between 0.07 and 0.16. Therefore, as fan aspect ratio decreases (or the fan becomes smaller), both flow rate and pressure coefficient are significantly reduced at a constant rotational speed although an associated drop in power consumption can be achieved.

Moreover, it has been reported that the traditional fan scaling laws are not effective to predict the flow characteristics of miniature centrifugal fans at low Reynolds number flows due to increased viscous effects [3]. Indeed, as the fan becomes smaller and operates at low rotational speeds, the boundary layers created on the fan rotors at low flow regime effectively block the flow through the fan, reducing the flow rate, and causing significant losses in the fan performance and transduction efficiency [4]. Furthermore, design of miniature fan motors and rotors represents further challenges for reliable and practical implementation, due to the high manufacturing cost, limited rotational speed, and need to prevent bearing failure [5]. Among other emerging air cooling technologies proposed as alternatives to rotary fans such synthetic jets and piezoelectric fans, recent performance review and comparison study concluded that electrohydrodynamic (EHD) air movers have great potential to overcome the limitations of miniaturized mechanical means to induce air cooling in modern microelectronic applications [1]. With the advantage of no moving parts, EHD air pumps have silent operation, good reliability, flexibility in scale and design, and considerable flow production for effective heat removal on small-scale applications.

The operation of EHD airflow induced by corona discharge occurs when a high voltage is applied between a highly curved corona emitter electrode (usually wire or needle) and a grounded collecting surface electrode, creating an electric field gradient in the air gap across them. The enhanced electric field near the emitter electrode ionizes the surrounding air particles and the created ions move towards the collector of opposite charge under the influence of the electric field and electrostatic forces, transferring their momentum and energy to the neutral air molecules via collisions and inducing air movement known

as an ionic wind. A simple schematic diagram of an EHD airflow induced by a positive corona discharge is shown in **Fig. 1**.
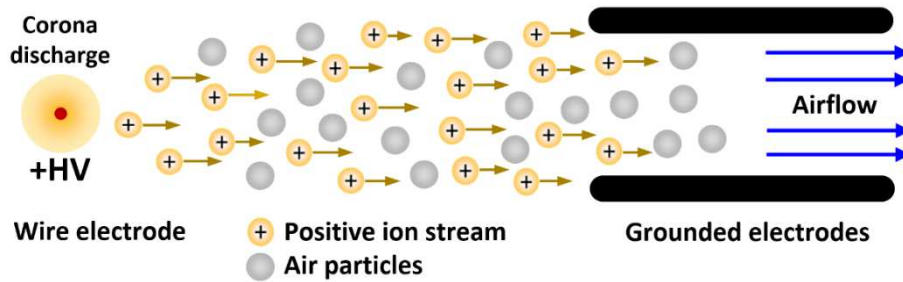

Fig. 1. Schematic diagram of an EHD airflow induced by a positive corona discharge.

EHD flow has been widely investigated using different electrode configurations either as air pumps to maximize flow generation, improve conversion efficiency, and evaluate the flow characteristics and velocity profile [6-11], or for forced convection heat transfer [12-15]. Moreover, EHD driven airflow provides another feature when it acts as a secondary flow to mix flows and modify the thermal boundary layer for heat transfer enhancements [16-19]. In the early 1960s, Robinson [20] presented one of earliest studies to examine the possibility of applying EHD driven flow for practical applications and concluded that EHD blowers have attractive advantages over conventional mechanical fans. Kalman et al. [21] were the first to study the optimization of a wire-to-plates EHD blower configuration and investigate its effectiveness as a cooling solution for electronic components. This study was extended later by Rashkovan et al. [22] to develop the optimization of the previous EHD blower and improve its performance.

However, it is only recently that the interest in employing EHD technology as an alternative cooling solution to rotary fans has increased for the applications of localized cooling of microelectronic components [23-25] and integration with heat sinks [26-28]. The first practical and successful integration of EHD air blower into a real-world electronic applications has been performed by Jewell-Larsen et al. in 2009 [29], who replaced a mechanical fan in a laptop (with a Thermal Design Power of 60 W) by a compact wire-to-plate EHD blower. The results of real operation demonstrated that a miniature EHD blower can offer promising cooling performance with lower installation size and acoustic levels compared with rotary fans. In their work to develop and optimize EHD blowers for practical applications, Jewell-Larsen et al. [30] identified the airflow performance scaling laws that predict the flow rate and static pressure of EHD devices based on the operating power and cross-sectional dimensions (width and height) of EHD blowers.

Due to the strong influence of the geometrical parameters of EHD devices on the corona discharge process and the resulting EHD flow, and in order to save cost and time, significant modelling efforts have been performed over the last decade to study the impact of design parameters and optimisation of

mesoscale EHD air pumps on the performance of flow generation or heat transfer characteristics [23, 31-35]. Very recently, Ramadhan et al. [36] presented a numerical study to optimise the configuration of miniature wire-to-plane EHD blower for a range of heights (from 2 to 10 mm) based on different operating conditions (voltage and power). Simple relations for each optimization method were determined to predict the optimal length and location of the collector electrode of each blower. Results of the static pressure and flow rate obtained by each optimized blower showed agreement with those predicted by the EHD scaling laws previously presented [30].

This work is established based on the results of the previous study [36] and is the first, to the authors' knowledge, to investigate the performance and the exit flow patterns of optimized miniature EHD blowers for practical applications. The investigation is considered with the focus on the key design factors, including device size, power consumption and generated flow rate. Two-dimensional (2D) and three-dimensional (3D) numerical models of the EHD airflows are developed and validated carefully against previous data. Based on thermal management considerations, an optimized combined EHD blower is proposed and comparisons, based on efficiency and performance, against commercial miniature rotary blowers are presented.

2. Numerical Modelling
2.1 EHD governing equations

The fundamental equations of EHD airflow that describe the interaction between the electric charges and the particle movement in the air can be given as following,

The electric field intensity ($\vec{E}$) created between the electrodes is described by Gauss's law,

$$\vec{\nabla}.\vec{E} = \frac{q}{\varepsilon_0} \tag{1}$$

where q is the space charge density (C/m³) and ε_0 is permittivity of free space (= 8.854×10^{-12} C/V.m). This can be defined in terms of the electric potential, V, by

$$\vec{E} = -\vec{\nabla}V \tag{2}$$

The electric potential in the air is governed by Poisson's equation, which can be obtained by substituting (2) into (1),

$$\vec{\nabla}.\vec{E} = -\nabla^2 V = \frac{q}{\varepsilon_0} \tag{3}$$

The equation that couples the electrostatic and Navier-Stokes equations for the airflow is derived by combining the following three equations:

i. The electric current density equation,

$$\vec{J} = \mu_\text{p}\vec{E}q + \vec{U}q - D\,\vec{\nabla}q \tag{4}$$

where μ_p is the air ion mobility in the electric field (m²/V.s), $\vec{U}$ is the velocity vector of airflow, D is the diffusivity coefficient of ions (m²/s). The three terms on the right side of equation (4) represent the charge conduction (the ion movement due to the electric field), charge convection (transport of charges by the airflow), and charge diffusion, respectively [37].

ii. The continuity equation for the electric current,

$$\vec{\nabla}.\vec{J} = 0 \tag{5}$$

iii. The conservation of mass equation,

$$\vec{\nabla}.\vec{U} = 0 \tag{6}$$

Combining equations (4) and (5) and using the continuity equation (6) gives the charge transport equation:

$$\vec{\nabla}.\left(\mu_\text{p}\,\vec{E}q - D\,\vec{\nabla}q\right) + \vec{U}.\vec{\nabla}q = 0 \tag{7}$$

Since the value of the air velocity ($\vec{U}$), which represents the charge convection term in equation (7), is very small compared with the drift velocity of ions ($\mu_\text{p}\vec{E}$) in the charge conduction term, it can be neglected [14]. The charge diffusion coefficient is included in (7) with a constant value although its effect on the numerical accuracy is relatively negligible [38]. The Navier-Stokes equations and continuity equation (6) describe the hydrodynamic part of the model for the steady state incompressible airflow under the effect of the electrostatic force,

$$\rho\vec{U}\,.\,\vec{\nabla}\vec{U} = -\vec{\nabla}p + \mu\,\nabla^2\vec{U} + q\vec{E} \tag{8}$$

where ρ is the air density (kg/m³), p is the air pressure (Pa), μ is the air dynamic viscosity (Ns/m²), and the term of $q\vec{E}$ represents the body or Coulomb force (N/m³).

The coupled equations for the electric field (3), charge transport (7), and airflow (6 and 8), were solved using the commercial package, COMSOL Multiphysics (V5.1), a partial differential equations solver based on the finite element method. The 3D modelling of EHD flow was solved using a high performance computing server (POLARIS) at the University of Leeds.

2.2. Validation of the numerical method

2.2.1. Solution domain and boundary conditions

The accuracy of the numerical method performed in this paper for the 3D model is validated against ranges of experimental and numerical data of a wire-to-plane EHD channel presented in [30], whereas the 2D validation results for the airflow rate and static pressure were reported in detail in [36]. A cross-section of the EHD channel geometry used in the validation of the 3D model is shown in **Fig. 2**, and the modelling parameters are listed in **Table 1**. In order to save computation time and minimize the large memory requirement for the 3D EHD flow models (up to 200 GB), symmetry boundary conditions were applied at the horizontal plane centered between the channel walls and at one of the channel sidewalls of the simulation domain. The numerical solution procedure and the boundary conditions applied to the present numerical model (summarized in **Table 2**) are adopted as described in [35, 36], including the assumptions for space charge generation. This is considered by applying Kaptsov's assumption [39] and using Peek's empirical formula [40] to estimate the electric field strength E_e created on the surface of a positive corona electrode.
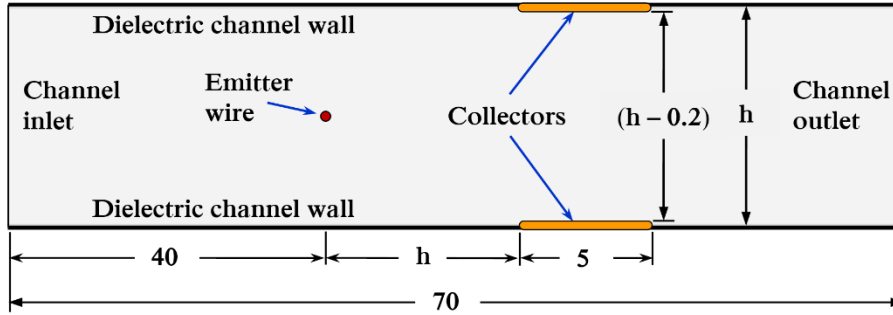

Fig. 2. Cross-section of the EHD channel geometry [30] used in the numerical validation. Dimensions in millimetres.

Table 1. Geometric parameters [30] and numerical modelling values used in the present validation model.

Parameter	Value
Applied potential, V_e	0 – 10 kV
The breakdown electric strength of air, E_0	3.23×10^6 V/m
Ion mobility coefficient, μ_p	2.1×10^{-4} m^2/V.s
Charge diffusion coefficient, D	5.3×10^{-5} m^2/s
Density of air, ρ	1.23 kg/m^3
Dynamic viscosity of air, μ	1.8×10^{-5} N.s/m^2
Corona wire radius, R_e	0.0125 mm
Channel height, h	2 , 6 mm
Channel length, L	70 mm
Channel width, w (= corona wire length)	100 mm
Horizontal distance between the electrodes, (= h)	2 , 6 mm
Collecting surface length	5 mm

Table 2. Boundary conditions used in the validation and developed numerical models.

Boundary	Electrostatics	Charge transport	Fluid dynamics
Corona wire electrode	$V = V_e$	$q = q_0$	No-slip ($U = 0$)
Collector electrode	Grounded ($V = 0$)	$q = 0$	No-slip ($U = 0$)
Dielectric channel walls	Neumann condition ($\partial V / \partial n = 0$)	Zero diffusive flux ($\partial q / \partial n = 0$)	No-slip ($U = 0$)
Channel inlet	($\partial V / \partial n = 0$)	($\partial q / \partial n = 0$)	Prescribed velocity [33, 35-37]
Channel outlet	($\partial V / \partial n = 0$)	($\partial q / \partial n = 0$)	$P = 0$
Air boundaries	($\partial V / \partial n = 0$)	($\partial q / \partial n = 0$)	Symmetry

A mesh independence study was performed for the flow in the upper half of the 3D simulation domain of 6 mm thick, 100 mm wide and 70 mm long, with increased mesh refinement near the corona and collecting electrodes, using three mesh levels with approximately 507550, 631000 and 757230 tetrahedral elements. Results revealed that the maximum difference in the value of the average air velocity at the blower outlet was approximately 0.6% between the two finest mesh densities. This demonstrated that the second mesh density, shown in **Fig. 3**, provides an acceptable balance between computational cost and solution accuracy.
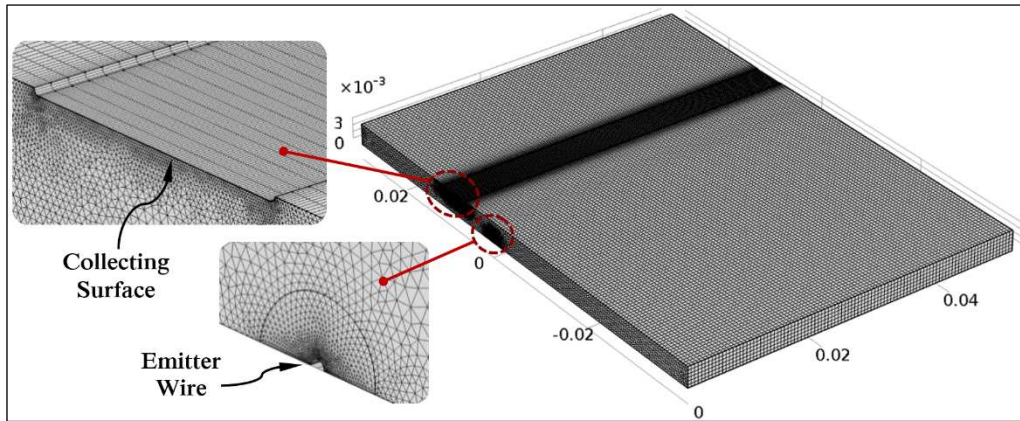

Fig. 3. Distribution of mesh element density for a half 3D domain of an EHD blower geometry with $h = 6$ mm and $w = 100$ mm, showing the mesh refinement at the emitter and the collector electrodes. Dimensions in metres.

2.2.2 Numerical validation results

The results of the 3D numerical solution are shown as volume map distributions in **Fig. 4**, which were generated at 1.5 W for a blower of height, length and width of 6 mm, 70 and 100 mm, respectively, showing the distributions of the electric potential, charge density, and air velocity generated through the channel. **Fig. 5** compares the mean outlet velocities of the present simulations against experimental data and numerical results presented in [30] for a range of input power. The results reveal that the average

discrepancies in the mean air velocities of the present 2D and 3D simulations are 9.2% and 5.4%, respectively, against the experimental data, showing good agreement and demonstrating the accuracy of the present numerical approach performed using COMSOL Multiphysics.
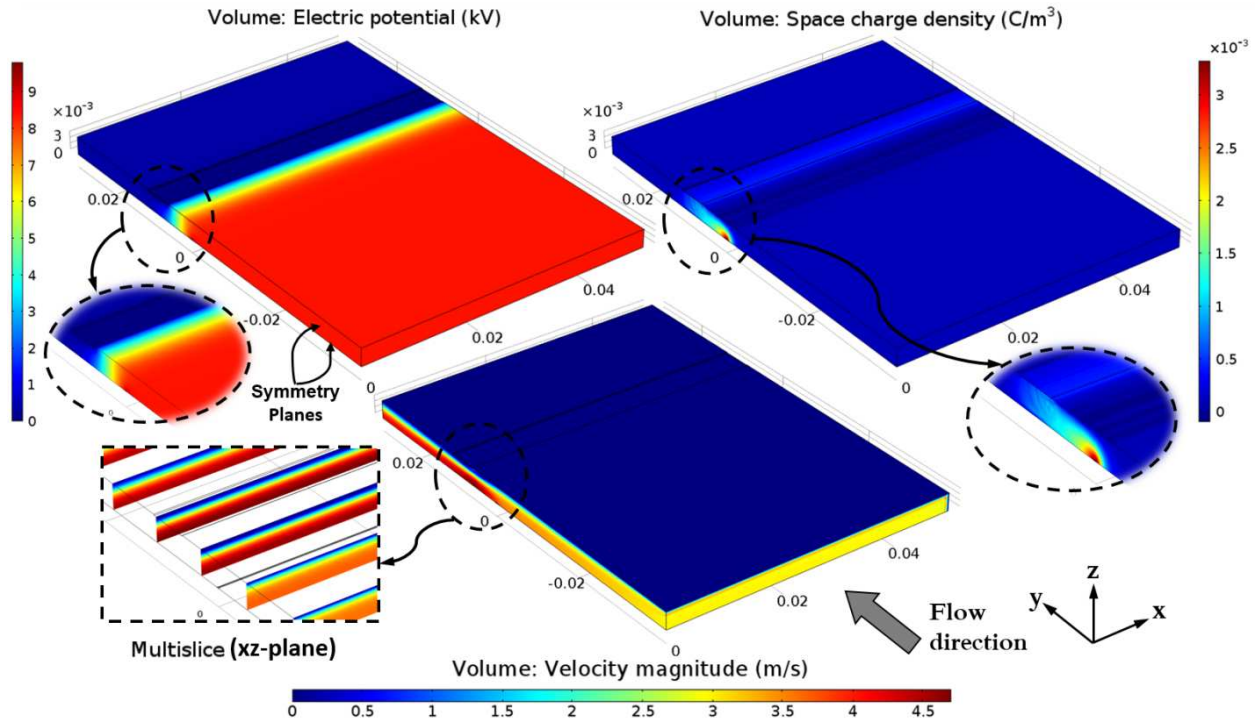
Fig. 4. Results of the 3D numerical solution as volume map distributions of a half of EHD channel generated at 1.5 W with 6 mm thick, 100 mm wide and 70 mm long, showing the distributions of: (at top-left) electric potential, (at top-right) space charge density, and (at bottom) air velocity. Dimensions in meters.

Fig. 5. Validation results of the mean outlet velocity generated by an EHD blower of $h = 6$ mm, $w = 100$ mm and $L = 70$ mm, for a range of operating power.

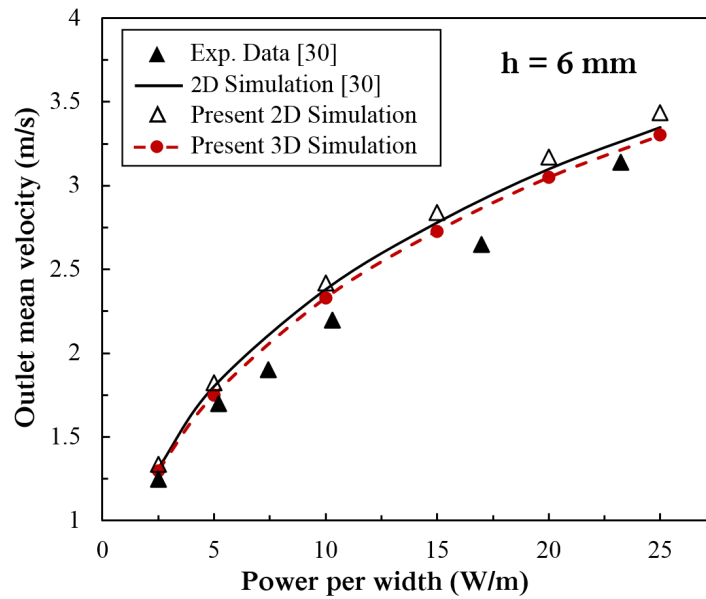## 2.3 Numerical configuration domain

The EHD blower geometry used in the present study is shown in **Fig. 6**. It is considered based on the optimal design parameters presented in [36], which are defined by

$$G_{\mathrm{P}} = (h/4) + 0.5 \tag{9}$$

$$b_{\mathrm{P}} = 1.5\,h \tag{10}$$

where G_{P} is the optimal electrode gap (mm), b_{P} is the maximum effective length of the collector (mm), (each for the case of constant input power), and h is the blower height (from 2 to 10 mm). The same modelling values used in the validation model are adopted, whereas the geometric parameters of the present EHD blower configuration are detailed in **Table 3**. The present work aims to highlight the advantages and characteristics of miniature EHD pumps, compared to commercial rotary blowers, for real-world thermal management applications. In order to improve the performance of optimized miniature EHD air blowers, the key design factors, including the installation size, limitations of the operating power and applied potential, and required cooling flow rate, are consid0ered.
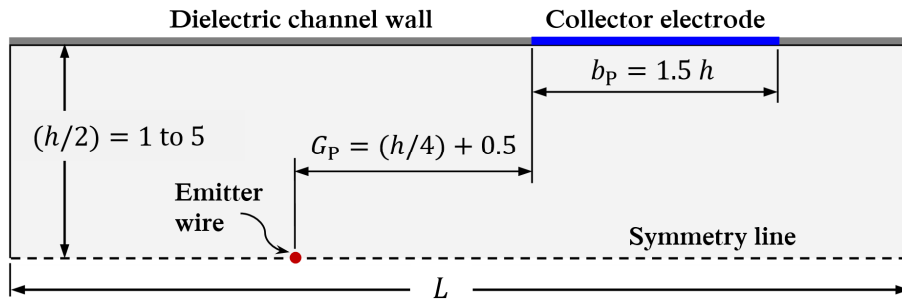
Fig. 6. Half domain of the EHD blower geometry used in the present study [36]. Dimensions in millimetres.

Table 3. Geometric parameters considered in the present study.

Geometric parameter	Value
Corona wire diameter, d	0.025 mm
Channel length, L	12 – 20 mm
Channel height, h	2 – 10 mm
Channel width, w	10 – 60 mm
Horizontal distance between electrodes, G_{P}	$= [(h/4) + 0.5]$, mm
Collecting surface length, b_{P}	$= [1.5\,h]$, mm

3. Results and Discussion

3.1 Influence of blower width

This section discusses the impact of the blower sidewalls on the air velocity profile and magnitude for a range of channel widths. It also studies the accuracy of the 2D numerical models to predict flow rates compared to the 3D modelling, where the friction losses due to channel sidewalls are included. To the authors' knowledge, this is the first 3D numerical investigation of the impact of the channel sidewalls on the flow characteristics for narrow EHD ducts, although the 2D simulation of EHD flow performed in previous studies has shown acceptable agreement against experimental data for wide flow channels. Due to limitations caused by the large solution memory required for the 3D modelling of thick domains (thicker than 6 mm), only blowers of $h = 2$ and 6 mm are considered in the present investigation. The optimal location and length of the collecting surface were assigned according to equations (9) and (10), whereas the length of each blower was reduced to 20 mm and the blower width was varied between 10 and 60 mm.

Fig. 7 illustrates the effect of the channel sidewalls on the outlet average velocity generated by each EHD blower at a fixed operating voltage that corresponds to 15 W/m input power used in the 2D simulation, showing the percentage decrease in the velocity magnitude for each blower width compared to that predicted by the 2D simulation. It is important to mention that fixing the operating voltage ensures that the generated air velocity through each blower remains constant regardless of the blower width, and any change in its magnitude is only caused by sidewall effects. Although there are slight differences between the values of percentage decrease at a given width of both blowers, the actual impact of the flow losses are different and can be determined based on the blower aspect ratio, which is defined by the ratio of the blower height to its width (h/w). For instance, the blower of $h = 2$ mm with an aspect ratio of 0.2 (at $w = 10$ mm), leads to a reduction in the velocity by 5.5% lower than that predicted by the 2D simulation, compared to an approximately 3% reduction for a blower of equivalent aspect ratio with $h = 6$ mm and $w = 30$ mm. However, the figures demonstrate that the influence of the flow resistance through shortened and thin EHD blowers decreases and can be neglected as the blower becomes wider (or the aspect ratio decreases). This indicates that using 2D modeling for short and wide EHD blowers is valid to predict flow rates effectively compared to that obtained by the means of the 3D simulation.

The results of the 3D numerical solution for the velocity distribution through narrow and wide EHD blowers with $h = 2$ and 6 mm are displayed in **Fig. 8**, showing that the induced flow at the exit of both blowers has uniform velocity gradient and the impact of flow resistance is insignificant.
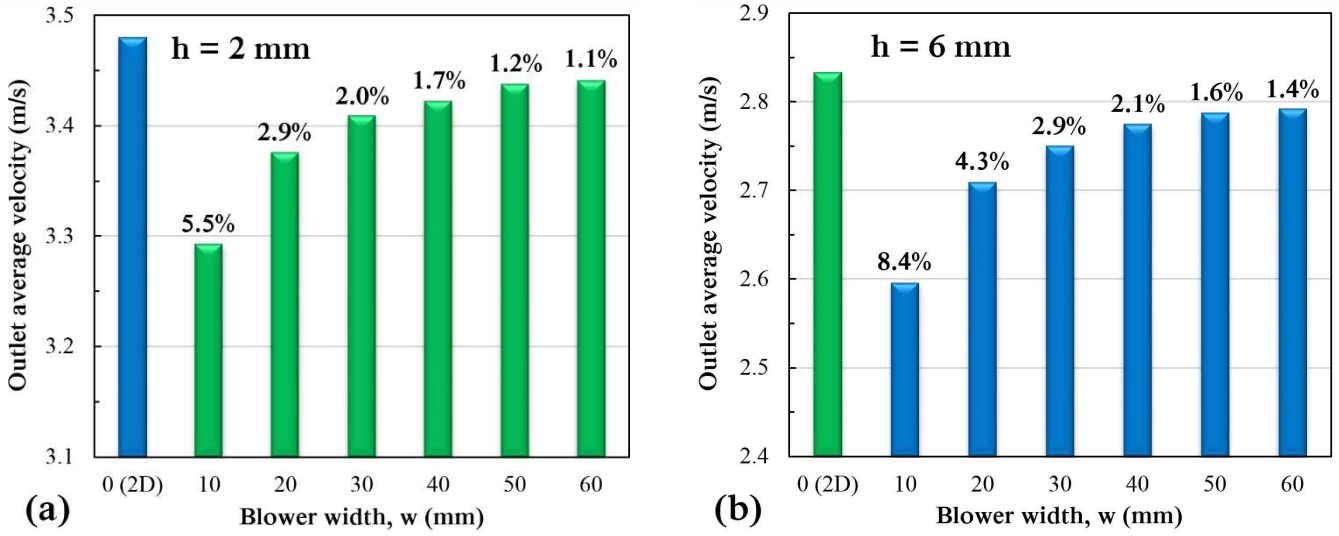
Fig. 7. Influence of blower width on the average outlet velocity generated in 3D modelling at a fixed operating voltage, showing the percentage decrease in the velocity magnitudes compared to the 2D results for optimized blowers of (a) $h = 2$ mm at ≈ 3.9 kV, and (b) $h = 6$ mm at ≈ 5.7 kV, each with 20 mm long.
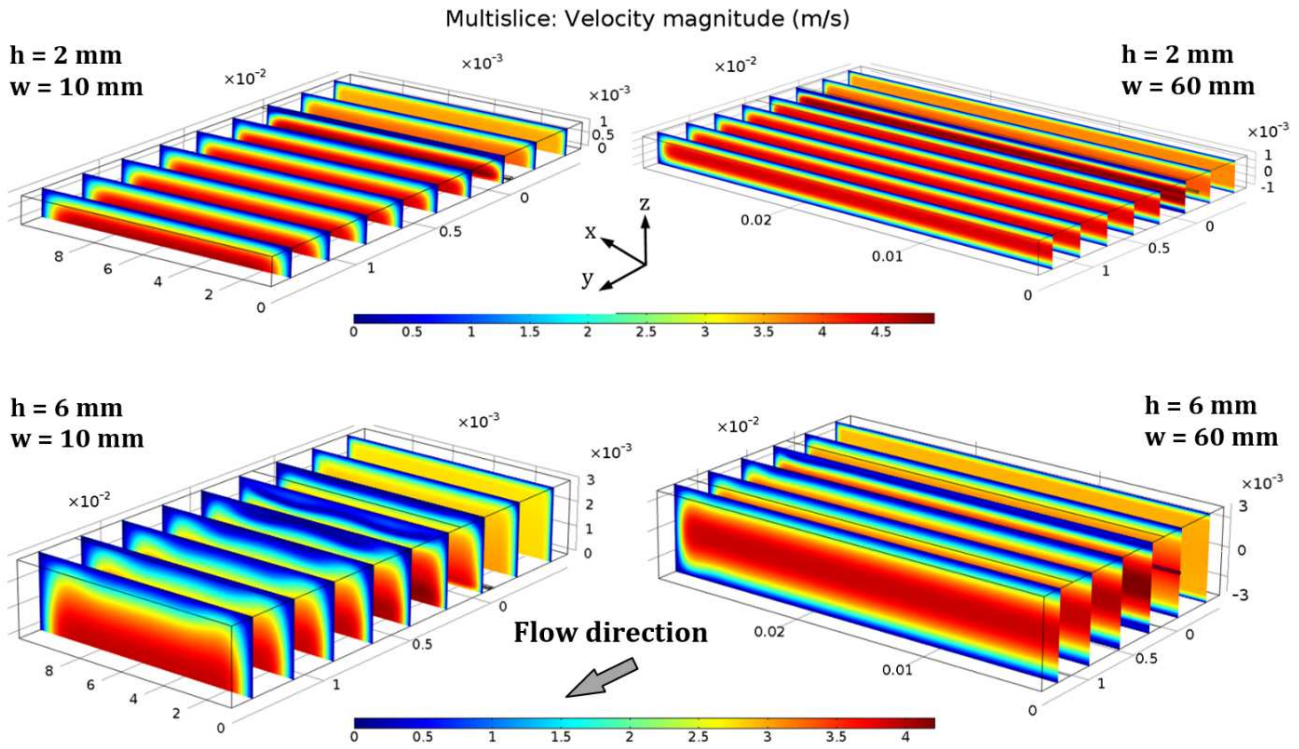
Fig. 8. Velocity distribution induced at a fixed operating voltage that corresponds to 15 W/m, through narrow and wide optimized EHD blowers for $h = 2$ mm (top) and $h = 6$ mm (bottom). Dimensions in metres.

Fig. 9 shows that the outlet velocity profile is uniform and has a parabolic distribution along the vertical y-z plane (at $x = 30$ mm) for the both wide blowers considered in **Fig. 8**, based on the coordinate system shown in **Fig. 10**.
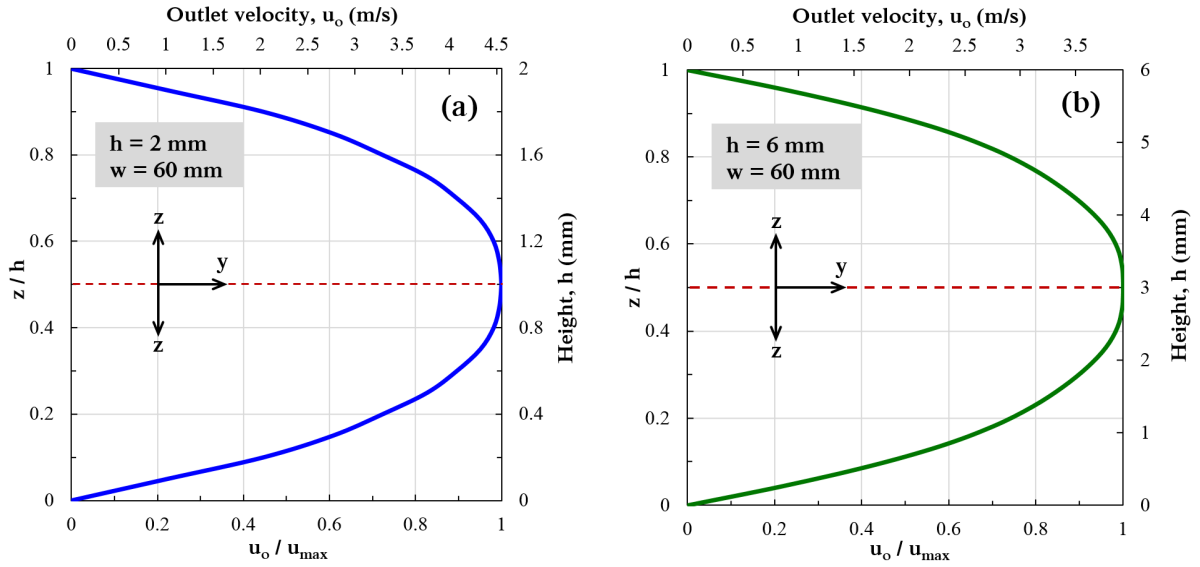
11

Fig. 9. Normalized velocity profiles in the central vertical *y-z* plane (at *x* = *w*/2), along the blower outlet of (a) *h* = 2 mm and (b) *h* = 6 mm.
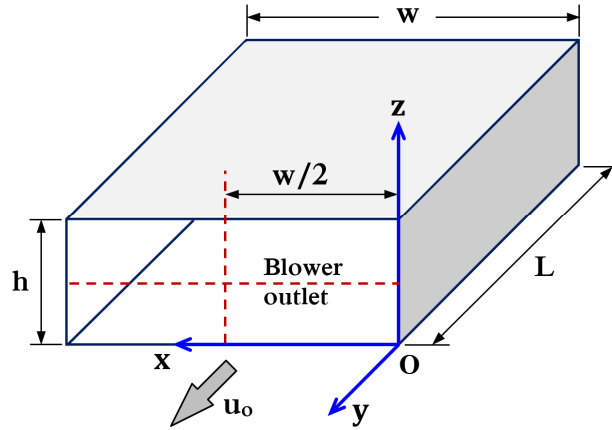

Fig. 10. Schematic diagram of the rectangular EHD blower's coordinate system.

Fig. 11 shows the velocity distribution on different *x-y* planes along the blower width for the two blowers considered here. For the thinner blower of *h* = 2 mm, it can be seen that the outlet velocity profile is similar (flat) for all selected planes (at *z* = 0.25, 0.5 and 1 mm), whereas the velocity magnitude is affected by the friction losses at the sidewalls (along the *x*-axis) and the bottom and upper walls (along the *z*-axis) of the blower, as shown in figures 10(a) and (b). The same behaviour is observed for the thicker blower of *h* = 6 mm, but with a slight disruption in the top-hat profile at the regions close to the upper and bottom walls (*z* = 0.5 and 1 mm), as shown in figures 10(c) and (d). This can be attributed to the impact of the electric field distribution caused by the increase in the vertical components of the Coulomb force as the blower becomes thicker [36].

In order to highlight that EHD blowers produce a uniform velocity profile, their flow pattern is compared with that produced by rotary fans, as presented in [41]. **Fig. 12** shows experimental measurements of air velocity distribution at the exit flow region of a centrifugal fan of diameter and height

of 60 mm and 11 mm, respectively. It can be clearly observed that the velocity profile of the airflow induced by rotary air movers is highly non-uniform, which is due to the non-uniform distribution of the static pressure on the fan impellers.

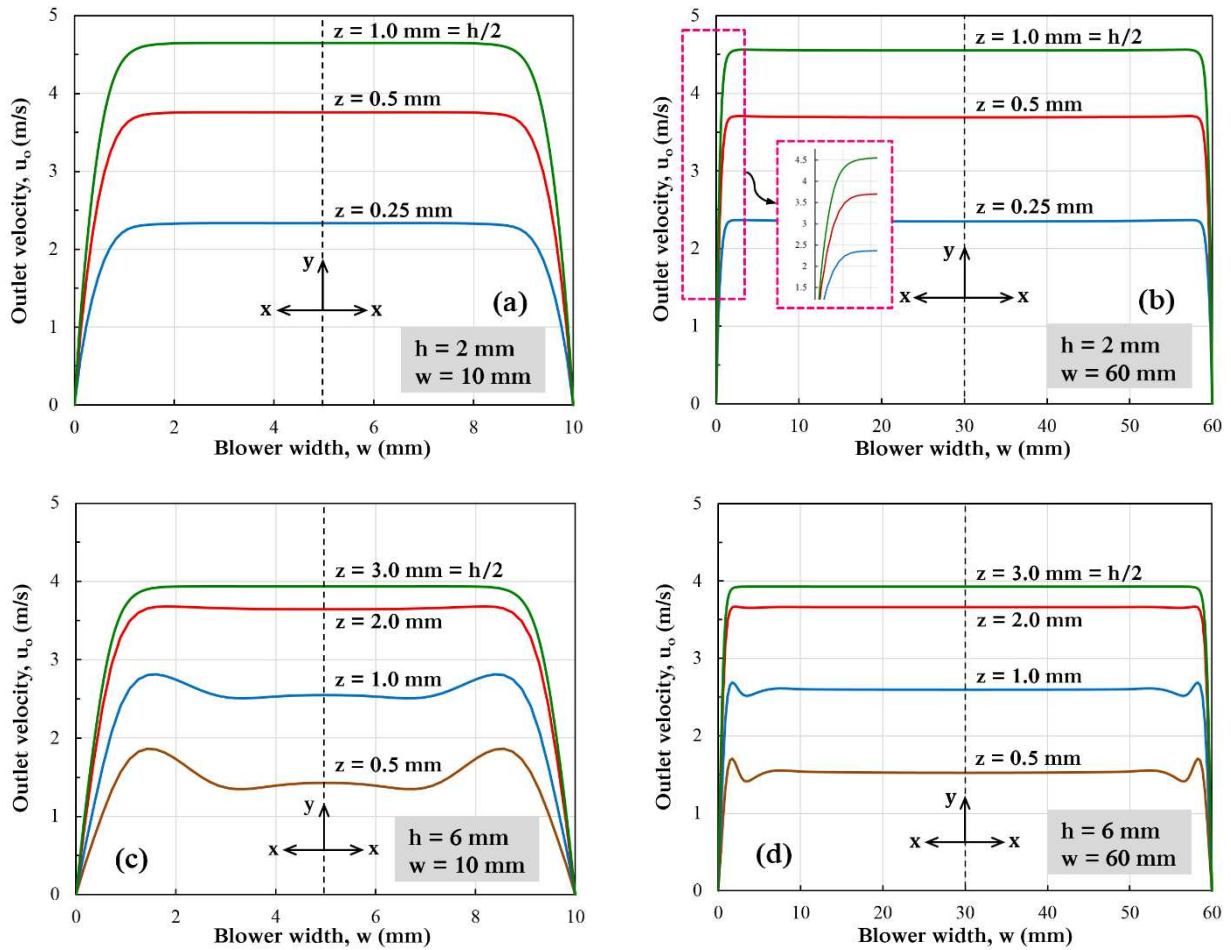**Fig. 11.** Velocity profile at the blower outlet in the *x-y* plane, for different widths of the blowers of *h* = 2 and 6 mm.
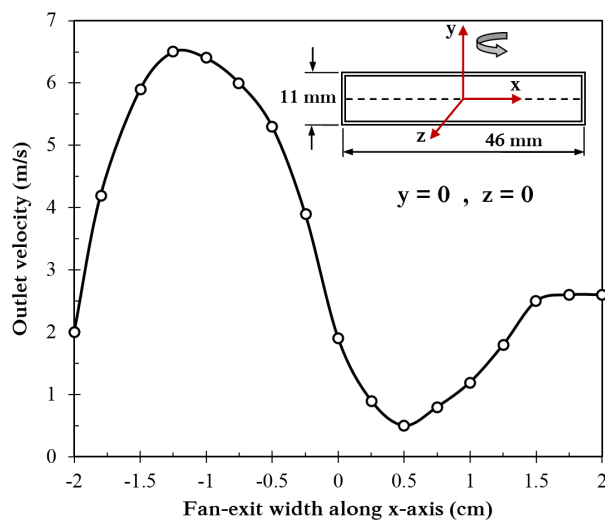

Fig. 12. Distribution of outlet velocity on the *x-z* plane at the exit region of a centrifugal rotary fan at 3100 rpm [41].

In a wire-to-plane EHD channels, the blower width is usually equal to the emitter wire length, and therefore, it can be employed to control the flow rate, static pressure, produced velocity and operating voltage. An EHD blower with 4 mm thickness and 15 mm length was modelled in 2D simulations at a fixed power of 0.5 W to demonstrate these relations.

The electrostatic pressure created due to the body force, which acts on the collecting surface and equals the channel static pressure, can be calculated by integrating the body force within the distance between the electrodes [30, 42]. The pressure at any point (z) along the electrode gap, G, for an EHD wire-to-plane configuration is given as [42],

$$\Delta P = \int_{z}^{G} qE \, \mathrm{d}z \tag{11}$$

where q and E ($= |\vec{E}|$) are respectively the charge density and the electric field strength within the electrode gap.

Fig. 13(a) shows how the pressure decreases and the flow rate increases as the blower becomes wider or the wire extends at a fixed input power. This behaviour is attributed to the reductions in the operating voltage and the electric field (or the body force) created across the electrodes, leading to reduced air velocities, as shown in **Fig. 13**(b). In this case, the increase in the ion current required for keeping the input power at a fixed level is due to the increase in the wire length. This can be explained based on the definition of the ion current,

$$I_c = (\mu_p Eq) \, A_w \tag{12}$$

where A_w is the surface area of the corona wire (m^2). Since the ion mobility is assumed constant and both the applied voltage and electric field strength decrease in this case, thus the ion current increases as A_w increases.

Practically, this trend is attractive for cooling extended heated surfaces such as heat sinks, where higher flow rates using lower operating voltages are required. Furthermore, the wire length can provide an additional useful degree of freedom by representing the EHD blowers in P-Q curves, which are usually used for rotary fans, to reflect their specifications based on static pressure (P) and generated flow rate (Q), as shown in **Fig. 13**(c).

For EHD devices of a wire-to-plane channel configuration, Larsen et al. [29] stated that both the static pressure P and outlet velocity u_o are functions of power per wire length. They demonstrated that the static pressure changes proportionally to (*Power*)$^{2/3}$, while the average velocity is proportional to (*Power*)$^{1/3}$. **Fig. 13** shows that the current predicted trends of static pressure and outlet average velocity

change proportionally against the blower width *w* at a fixed operating power, and agree very well with those obtained from scaling relations presented in [29], which are identified by dashed lines in figures (a) and (b).
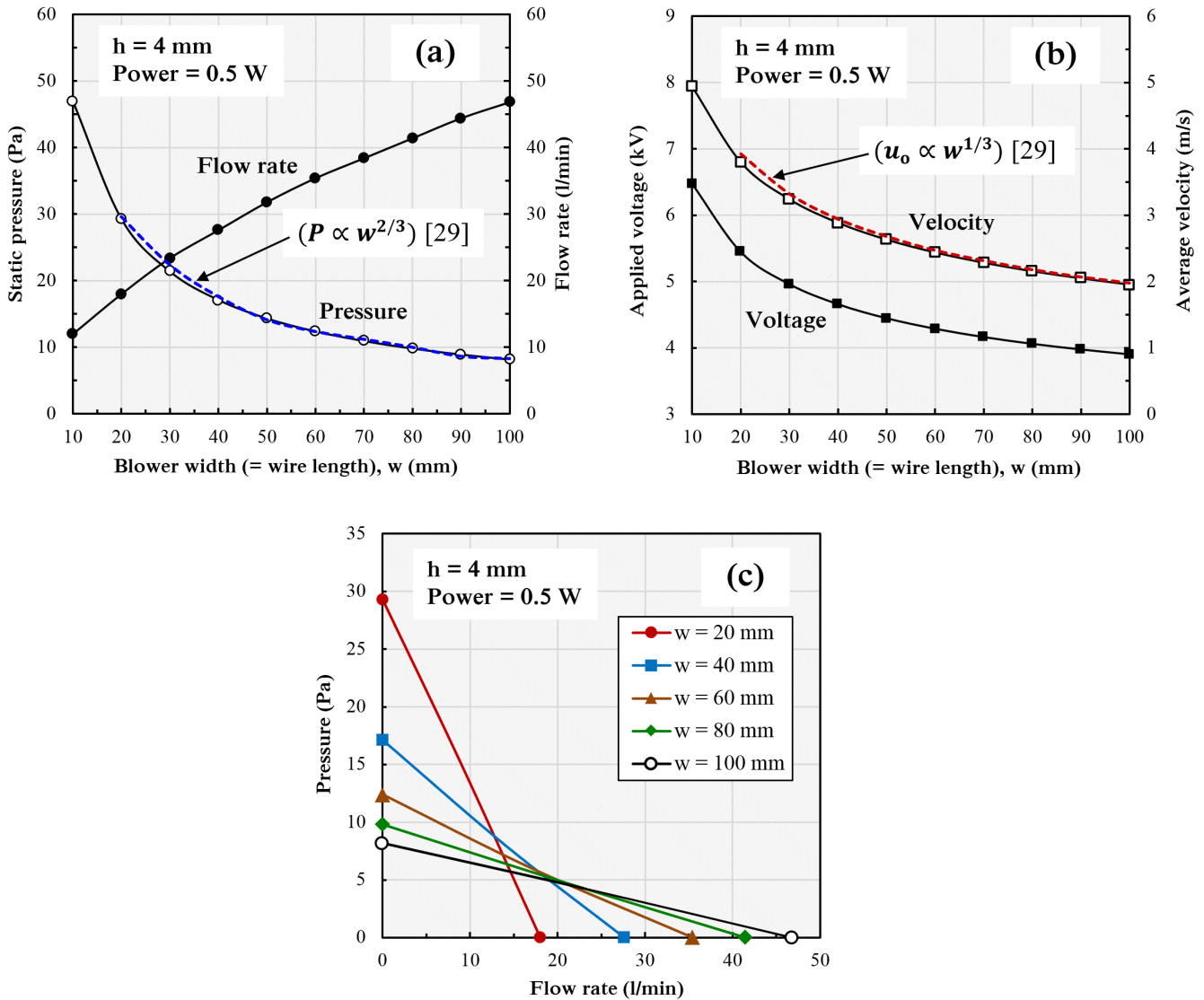

Fig. 13. Effect of the blower width (or the emitter wire length) on (a) static pressure and flow rate, (b) outlet average velocity and applied voltage, and (c) fan P-Q curves, for a blower of *h* = 4 mm operated at 0.5 W.

3.2 Combined EHD blowers

In the practical applications, EHD blowers are usually designed to fit the limited thickness of the electronic device, regardless if the used blower height is not the most efficient one compared to other levels of blower heights at a given operating power. **Fig. 14**(a) shows the average outlet velocity as a function of input power for different optimized blowers of length 20 mm. It can be seen that the average velocities generated by thinner blowers are higher than those obtained by thicker ones at a given input power. However, although the expected airflow rates produced by the thicker blowers are higher, the applied potential required to fix the power at a certain level increases as the blower becomes thicker, as

shown in **Fig. 14**(b). Typically, reducing the blower height at a given wire length and fixed input power leads to a higher air velocity, lower operating voltage, and reduced installation size, meeting the thermal management requirements for cooling thin microelectronics. Based on this fact and in order to balance these related factors, an EHD blower of two combined thin channels are developed and compared with a blower of an equivalent height at a fixed operating power.
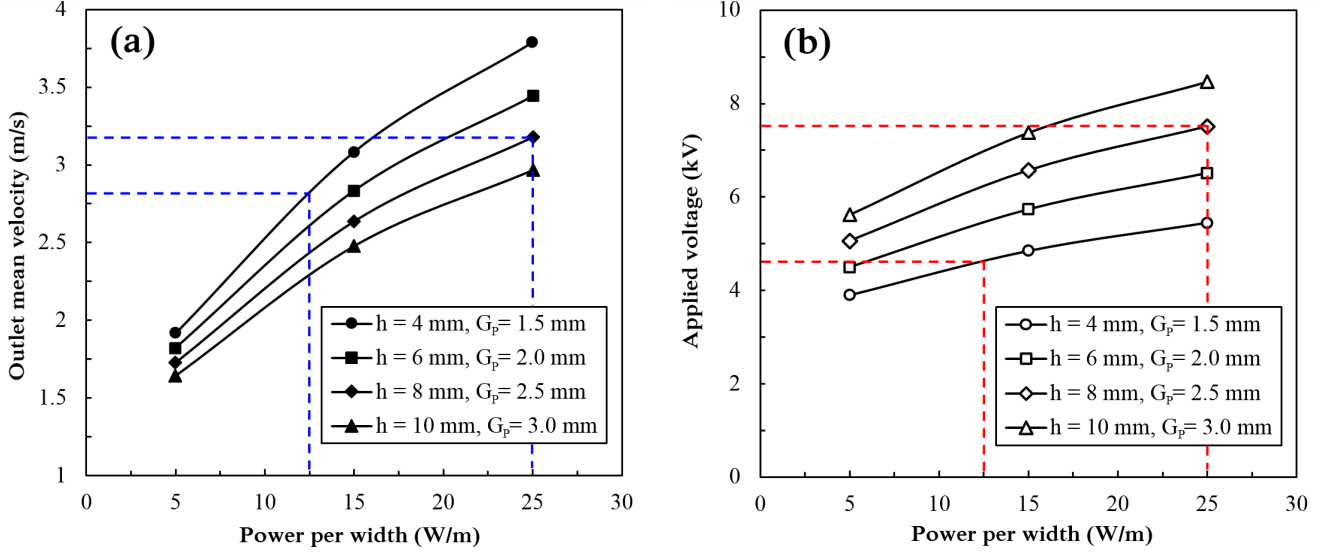

Fig. 14. Operating input power as a function of (a) average outlet velocity, and (b) required applied voltage, for different optimized EHD blowers [36].

Two EHD blowers, each with 4 mm thickness and optimal design parameters ($G_P = 1.5$ mm and $b_P = 6$ mm), are combined, forming an integrated blower of 8 mm thickness. In order to reduce the friction losses of the EHD-driven flow, the middle wall separating the two thin channels (located downstream of the collector) is removed, while the wall located upstream of the collector is kept to avoid electric field interference. The combined blower is operated at an overall power of 25 W/m, which is divided equally between the thin channels each with 12.5 W/m, and the generated airflow velocity is compared with that generated by an optimized blower of $h = 8$ mm ($G_P = 2.5$ mm and $b_P = 12$ mm), using the same total operating power.

The predicted distributions of the air velocity generated by both blowers are shown in **Fig. 15**. The results demonstrate that the combined blower of two 4mm-channels is able to produce an outlet average air velocity up to approximately 3 m/s, which is a little higher than that identified by a blue dashed line in **Fig. 14**(a) for a blower of $h = 4$ mm at 12.5 W/m due to the reduced friction losses, and is very close to that obtained by the blower of $h = 8$ mm (3.2 m/s). This indicates that the combined blower has almost the same pumping efficiency of that of $h = 8$ mm, consuming the same total electrical power but with a reduced operating voltage by approximately 3 kV (39%), as shown with red dashed lines in **Fig. 14**(b).
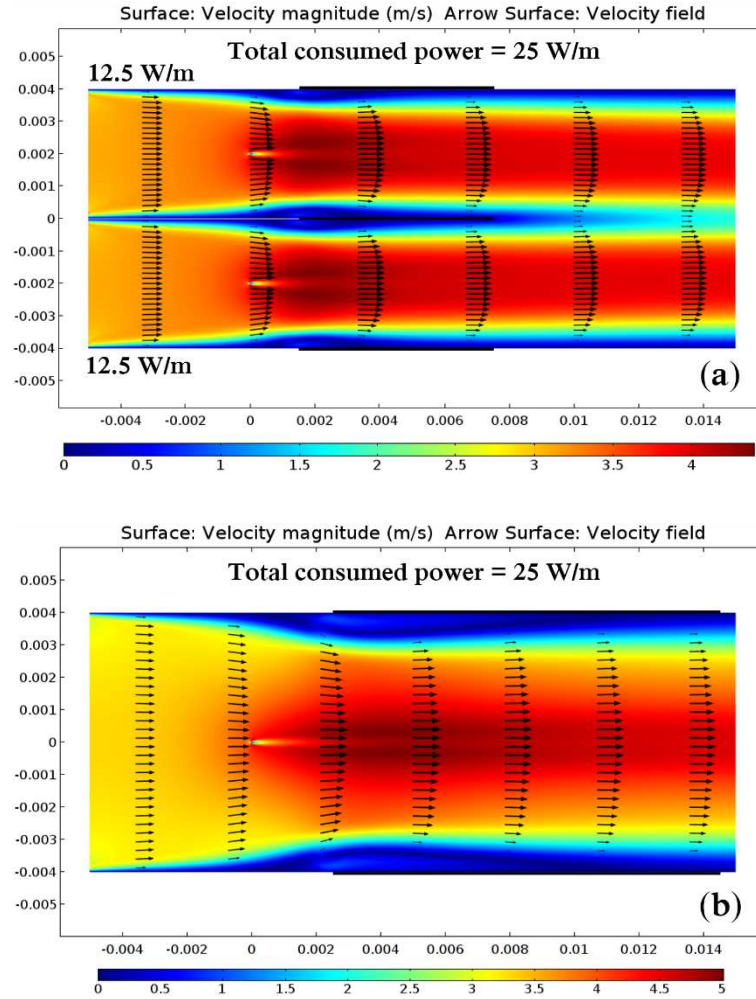
Fig. 15. Distribution of air velocity generated at 25 W/m through (a) combined EHD blower of two 4 mm-thick channels, and (b) an EHD blower with h = 8 mm. Dimensions in metres.

Table 4 compares different EHD blowers generated at 2.5 W, each of 100 mm width, showing that the combined blower has the best performance among others due to its relatively high flow rate produced using a low operating voltage. In addition, due to the shorter length of the collectors used in the combined blower (6 mm each), the length (or the overall size) of the new blower can be reduced further compared to those of the blower of h = 8 mm (12 mm). Moreover, the new blower offers an improved outlet velocity profile with two high stream paths, which is highly beneficial for cooling specific electronic components.

Table 4. Comparison of airflow rate generated at 2.5 W by different EHD blowers, each of 100 mm width and 20 mm length.

Trend	Blower height, h (mm)	Optimal collector length, b_P (mm)	Electrode gap, G_P (mm)	Operating voltage (kV)	Flow rate	
					l/min	CFM
(**a**)	4	6	1.5	**5.4**	91	3.21
(**b**)	6	9	2.0	6.5	124	4.37
(**c**)	8	**12**	2.5	**7.5**	**152**	5.39
(**d**)	10	15	3.0	8.4	178	6.28
(**e**)	8 (Combined)	**6**	1.5	**4.6**	**143**	5.03

Fig. 16 illustrates the curves of static pressure against airflow rate generated at 2.5 W by the EHD blowers listed in **Table 4**. The trends from (a) to (d) in the figure reveal that the flow rate decreases as the blower height is reduced at a fixed blower width while the static pressure increases. Indeed, as the blower becomes thinner at a given operating power, both the horizontal (G_P) and vertical (height parameter) electrode gaps decrease, increasing the electric field strength created across the electrodes. Unlike the case explained using equation (12) in the previous section, both the electric field and the ion current increase here due to the reduction in the electrode gap at a fixed wire length, which improves the body force and leads to a higher pressure head.

For the combined blower (e), the thin EHD channels that have small electrode gaps and a shared outlet area can create high electric fields and contribute together to generate the total flow rate and pressure head of the combined blower, which (the total pressure) is found to be higher compared to that of the blower (a) although they have the same electrode gap and consume equal total power. This can be attributed to the level of applied voltage required to fix the input power at a certain level in both blowers (a and e), as listed in **Table 4**, which highly affects the electric field strength and its distribution along the collecting surfaces. It is found that the change in the static pressure generated by a single channel of the combined blower (at 12.5 W/m) and that of the blower (a) (at 25 W/m) confirms the relationship between the static pressure and input power reported in [29, 30] for ideal EHD devices, which suggests that $\Delta P \propto$ Power$^{2/3}$. The total static pressure of the combined blower is calculated following the relation given in [29], which states that a multi-stage EHD device operated by a number of wires (N) at a reduced electric field interference has N times the static pressure of a single wire device.
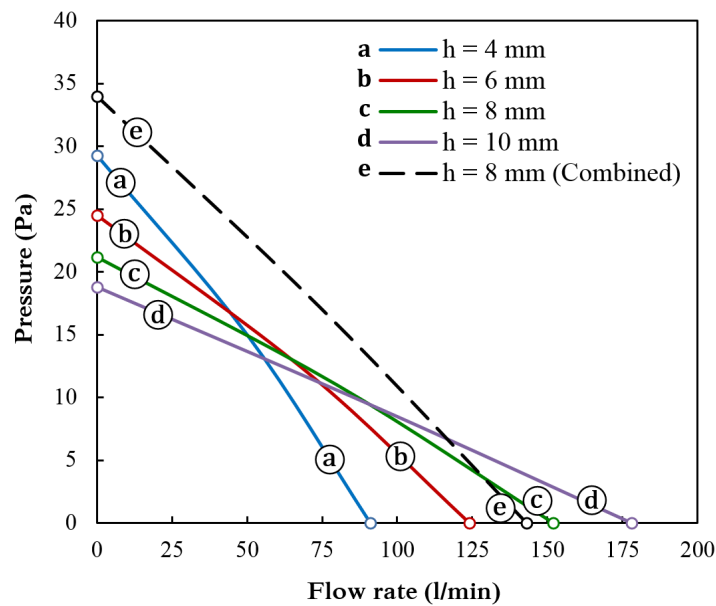

Fig. 16. Fan P-Q curves of different EHD blowers generated at 2.5 W, each of w = 100 mm.

The combined blower can provide another important advantage when it is used as a flow-controlled cooling system in thermal management applications. In this case, the flow velocity generated by the combined blower can be controlled by changing the operating power supplied to each of its channels, depending on the local cooling rate required for the application. **Fig. 17** shows the simulation results of a flow-controlled EHD blower at 25 W/m total power, which is consumed differently with 10 and 15 W/m by the upper and bottom channels, respectively. Both the average outlet velocity and the flow rate are kept constant but a different velocity profile along the blower outlet is achieved. It is useful to bear in mind that the presented combined EHD blower of two 4-mm channels was developed as an example, and further developments for other thicknesses with more than two thin channels can also be investigated.
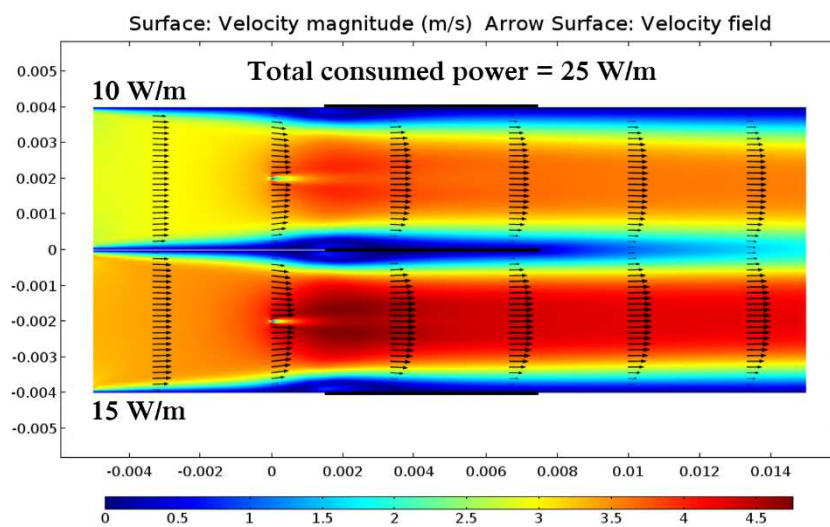

Fig. 17. Distribution of air velocity through a flow-controlled combined EHD blower generated at 25 W/m. Dimensions in metres.

3.3 Comparisons against rotary blowers

This section presents a comparison of the performance of miniature EHD blowers and mechanical centrifugal fans. The results of 3D simulations developed for thin EHD blowers of 3 mm thickness and 12 mm length were compared with equivalent commercial rotary blowers provided by SUNON Inc. [43], based on blower size, power consumption and flow rate production, as illustrated in **Table 5**. It can be observed that the EHD air movers are more competitive as cooling solutions than the conventional blowers for miniaturized applications and extended heated surfaces. Unlike traditional rotary blowers, the reduction or extension of the height and width of the EHD blowers are independent of the device length, offering flexible fabrication for the blower structure to fit limited spaces or extended heated components, whereas the rotary blowers are restricted by the circular rotation of the blades.

For example, at a fixed blower width, the EHD blower (g) can produce approximately the same flow rate of that provided by the rotary blower (a) with a slight increase in the power consumption but with a 60% reduction in the size. Moreover, increasing the operating power of the blower (f) by 0.14 W, over that

consumed by blower (a), leads to improvement in the flow rate with reduction of the size by approximately 37% and 33%, respectively, showing nearly similar efficiency with a gain in the width of 20 mm. Furthermore, the narrow EHD blower (j) shows higher efficiency than the rotary one (d) by more than 1050%, generating up to 75% higher airflow and a 180% reduction in electrical power, but with an increase in the device size by 48%. However, decreasing the length of the blower (j) to 8 mm can reduce its size to 240 mm^3, which is equivalent to that of (d).

Table 5. Comparison of characteristics of EHD blowers with 3 mm thickness modelled in 3D simulations at a range of operating voltage from 4 to 4.3 kV, against those of mechanical blowers of the same height presented by SUNON [43].

Blower Type		Width, w (mm)	Length, L (mm)	Size (mm³)	Consumed Power (W)	Flow Rate, Q (l/min)	Flow Rate, Q (CFM)	Transduction Efficiency (CFM/W)
Rotary Blowers	**(a)**	30	30	**2700**	**0.36**	**18**	**0.64**	1.78
	(b)	17	17	867	0.1	6.5	0.23	2.3
	(c)	12	12	432	0.1	2.67	0.094	0.94
	(d)	9	9	**243**	**0.28**	**1.17**	**0.0413**	**0.147**
EHD Blowers	**(e)**	50	12	1800	0.75	29.4	1.04	1.4
	(f)	50	12	**1800**	**0.5**	**24.6**	**0.87**	1.74
	(g)	30	12	**1080**	**0.45**	**17.4**	**0.614**	1.36
	(h)	30	12	1080	0.3	14.4	0.51	1.7
	(i)	20	12	720	0.2	9.6	0.34	1.7
	(j)	10	12	**360**	**0.1**	**4.8**	**0.17**	**1.7**

In addition to other merits that the EHD-driven flow devices have over the rotary blowers such as silent operation, and no vibration or moving parts, they have the further advantage of producing more uniform outlet velocity profiles across their width [29, 30], as shown in **Fig. 18**. This advantage offers active heat dissipation from narrow flow paths such as heat sink fin-channels, compared to the non-uniform outlet velocity profile obtained by mechanical blowers, especially when they are miniaturized.
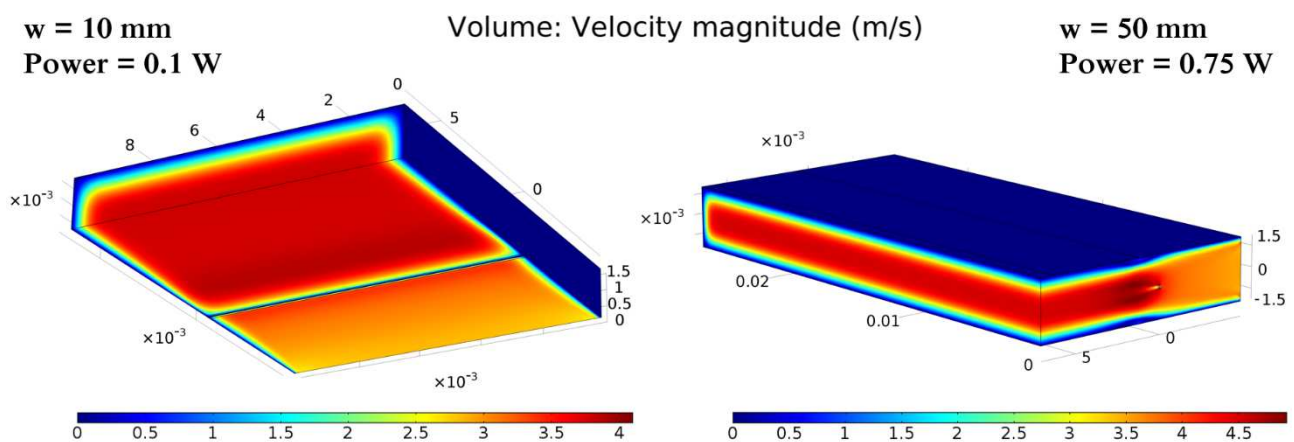

Fig. 18. Three-dimensional simulation results of EHD blower of 3 mm thickness with different widths and operating powers, showing a uniform outlet velocity profile. Dimensions in metres.

It is important to note also that the rotary blowers presented in this comparison are the thinnest blowers commercially available, according to the authors' knowledge, while further reduction in the miniature EHD blower size (with heights less than 2 mm and lengths less than 12 mm) is possible. However, the high voltage required to operate the EHD discharge still presents a practical challenge for using it to cool portable microelectronic devices such as laptops. In fact, the applied potential can be minimized for thin EHD blowers by using specific collector geometry, very fine emitter wire and optimized electrode gap. From a design and thermal management perspective, the balance between the key design factors, including the space available for the cooling system, the limitations of operating power, and the required cooling flow rate, is the key criteria for optimizing EHD devices for small-scale electronic applications. Once the balance between the aforementioned factors is determined, depending on the limitations and requirements of the application itself, design optimization and modification of the miniature EHD blowers can make them feasible alternatives to mechanical cooling solutions in real-world applications.

4. Conclusions

A numerical study to highlight the practical capabilities of miniature EHD air blowers is performed using both 2D and 3D numerical simulation methods that have been validated successfully against previous data. This study explores the performance and flow pattern of miniature EHD air blowers required in the practical implementation as thermal management cooling solutions. Based on blower width, investigation of the influence of the blower sidewalls on the flow characteristics shows that 2D simulations are valid for shortened and wide blower domains and can predict airflow rates generated accurately compared to that obtained using the 3D simulations. In order to minimize the operating voltage required to generate a certain flow rate, a configuration of two combined thin EHD blowers is developed and compared against other levels of blower height. Results reveal that the combined blower can produce flow rates close to that obtained by a blower of the same thickness, consuming the same electric power but with reducing the applied potential by approximately 40%. This can be exploited to provide further control of localized cooling in thermal management applications. A comparison against commercial rotary blowers demonstrates that the optimized miniature EHD blowers are more competitive for cooling miniaturized and extended heated surfaces based on blower size, uniform flow rate, and power consumption.

However, as is true of many other emerging technologies, EHD based cooling systems still require further research, development and design optimization, particularly to reduce the required operating voltages, before they can be adopted commercially for the thermal management of thin and small-scale electronic devices.

References

1. Wang, H.-C., N.E. Jewell-Larsen, and A.V. Mamishev, *Thermal management of microelectronics with electrostatic fluid accelerators.* Applied Thermal Engineering, 2013. **51**(1): p. 190-211.

2. Walsh, P., V. Egan, R. Grimes, and E. Walsh. *Scaling of Flow Characteristics and Power Consumption With Profile Height for Miniature Centrifugal Fans*. in *ASME 2007 5th International Conference on Nanochannels, Microchannels, and Minichannels*. 2007. American Society of Mechanical Engineers.

3. Day, S.W., P.P. Lemire, R.D. Flack, and J.C. McDaniel. *Effect of Reynolds Number on Performance of a Small Centrifugal Pump*. in *ASME/JSME 2003 4th Joint Fluids Summer Engineering Conference*. 2003. American Society of Mechanical Engineers.

4. Grimes, R., P. Walsh, E. Walsh, and V. Egan. *The Effects of Diameter and Rotational Speed on the Aerodynamic Performance of Low Profile Miniature Radial Flow Fans*. in *ASME 2007 5th International Conference on Nanochannels, Microchannels, and Minichannels*. 2007. American Society of Mechanical Engineers.

5. Rodgers, P., V. Eveloy, and M.G. Pecht. *Limits of air-cooling: Status and challenges*. in *Semiconductor Thermal Measurement and Management Symposium, 2005 IEEE Twenty First Annual IEEE*. 2005. IEEE.

6. Rickard, M., D. Dunn-Rankin, F. Weinberg, and F. Carleton, *Maximizing ion-driven gas flows.* Journal of Electrostatics, 2006. **64**(6): p. 368-376.

7. Moreau, E. and G. Touchard, *Enhancing the mechanical efficiency of electric wind in corona discharges.* Journal of Electrostatics, 2008. **66**(1): p. 39-44.

8. Moon, J.-D., D.-h. Hwang, and S.-T. Geum, *An EHD gas pump utilizing a ring/needle electrode.* IEEE Transactions on Dielectrics and Electrical Insulation, 2009. **16**(2): p. 352-358.

9. Colas, D.F., A. Ferret, D.Z. Pai, D.A. Lacoste, and C.O. Laux, *Ionic wind generation by a wire-cylinder-plate corona discharge in air at atmospheric pressure.* Journal of applied physics, 2010. **108**(10): p. 103306.

10. June, M.S., J. Kribs, and K.M. Lyons, *Measuring efficiency of positive and negative ionic wind devices for comparison to fans and blowers.* Journal of Electrostatics, 2011. **69**(4): p. 345-350.

11. Birhane, Y., S. Lin, and F. Lai, *Flow characteristics of a single stage EHD gas pump in circular tube.* Journal of Electrostatics, 2015. **76**: p. 8-17.

12. Marco, S. and H. Velkoff, *Effect of electrostatic fields on free-convection heat transfer from flat plates.* ASME Paper No. 63-HT-9, 1963.

13. Franke, M. and L. Hogue, *Electrostatic cooling of a horizontal cylinder.* Journal of heat transfer, 1991. **113**(3): p. 544-548.

14. Owsenek, B. and J. Seyed-Yagoobi, *Theoretical and experimental study of electrohydrodynamic heat transfer enhancement through wire-plate corona discharge.* Journal of Heat Transfer, 1997. **119**(3): p. 604-610.

15. Yonggang, Y., H. Junping, A. Zhongliang, Y. Lanjun, and Z. Qiaogen, *Experimental studies of the enhanced heat transfer from a heating vertical flat plate by ionic wind.* Plasma Science and Technology, 2006. **8**(6): p. 697.

16. Velkoff, H. and R. Godfrey, *Low-velocity heat transfer to a flat plate in the presence of a corona discharge in air.* Journal of Heat Transfer, 1979. **101**(1): p. 157-163.

17. Takimoto, A., Y. Tada, Y. Hayashi, and K. Yamada, *Convective heat-transfer enhancement by a corona discharge.* Heat Transfer-Japanese Research;(United States), 1991. **20**(1).

18. Shooshtari, A., M. Ohadi, and F.H. França. *Experimental and numerical analysis of electrohydrodynamic enhancement of heat transfer in air laminar channel flow*. in *Semiconductor Thermal Measurement and Management Symposium, 2003. Ninteenth Annual IEEE*. 2003. IEEE.

19. Go, D.B., R.A. Maturana, T.S. Fisher, and S.V. Garimella, *Enhancement of external forced convection by ionic wind.* International Journal of Heat and Mass Transfer, 2008. **51**(25): p. 6047-6053.

20. Robinson, M., *Movement of air in the electric wind of the corona discharge.* American Institute of Electrical Engineers, Part I: Communication and Electronics, Transactions of the, 1961. **80**(2): p. 143-150.

21. Kalman, H. and E. Sher, *Enhancement of heat transfer by means of a corona wind created by a wire electrode and confined wings assembly.* Applied Thermal Engineering, 2001. **21**(3): p. 265-282.

22. Rashkovan, A., E. Sher, and H. Kalman, *Experimental optimization of an electric blower by corona wind.* Applied Thermal Engineering, 2002. **22**(14): p. 1587-1599.

23. Go, D.B., S.V. Garimella, T.S. Fisher, and R.K. Mongia, *Ionic winds for locally enhanced cooling.* Journal of Applied Physics, 2007. **102**(5): p. 053302.

24. Go, D.B., R. Maturana, R.K. Mongia, S.V. Garimella, and T.S. Fisher. *Ionic Winds for Enhanced Cooling in Portable Platforms*. in *Electronics Packaging Technology Conference, 2008. EPTC 2008. 10th*. 2008. IEEE.

25. Hsu, C.-P., N.E. Jewell-Larsen, I.A. Krichtafovitch, and A.V. Mamishev, *Heat-transfer-enhancement measurement for microfabricated electrostatic fluid accelerators.* Journal of Microelectromechanical Systems, 2009. **18**(1): p. 111-118.

26. Schlitz, D. and V. Singhal. *An electro-aerodynamic solid-state fan and cooling system*. in *Semiconductor Thermal Measurement and Management Symposium, 2008. Semi-Therm 2008. Twenty-fourth Annual IEEE*. 2008. IEEE.

27. Huang, R.-T., W.-J. Sheu, and C.-C. Wang, *Heat transfer enhancement by needle-arrayed electrodes–An EHD integrated cooling system.* energy Conversion and Management, 2009. **50**(7): p. 1789-1796.

28. Gallandat, N. and J.R. Mayor, *Novel Heat Sink Design Utilizing Ionic Wind for Efficient Passive Thermal Management of Grid-Scale Power Routers.* Journal of Thermal Science and Engineering Applications, 2015. **7**(3): p. 031004.

29. Jewell-Larsen, N., H. Ran, Y. Zhang, M. Schwiebert, K.H. Tessera, and A. Mamishev. *Electrohydrodynamic (EHD) cooled laptop*. in *Semiconductor Thermal Measurement and Management Symposium, 2009. SEMI-THERM 2009. 25th Annual IEEE*. 2009. IEEE.

30. Jewell-Larsen, N.E., G.G. Joseph, and K.A. Honer. *Scaling laws for electrohydrodynamic air movers*. in *ASME/JSME 2011 8th Thermal Engineering Joint Conference*. 2011. American Society of Mechanical Engineers.

31. Jewell-Larsen, N., C. Hsu, I. Krichtafovitch, S. Montgomery, J. Dibene, and A.V. Mamishev, *CFD analysis of electrostatic fluid accelerators for forced convection cooling.* Dielectrics and Electrical Insulation, IEEE Transactions on, 2008. **15**(6): p. 1745-1753.

32. Ongkodjojo, A., D. Li, R.C. Roberts, Q. Liu, and N.C. Tien. *Modeling and measurement of microfabricated corona discharge structures*. in *Nano/Micro Engineered and Molecular Systems, 2008. NEMS 2008. 3rd IEEE International Conference on*. 2008. IEEE.

33. Jewell-Larsen, N.E., S.V. Karpov, I.A. Krichtafovitch, V. Jayanty, C.-P. Hsu, and A.V. Mamishev. *Modeling of corona-induced electrohydrodynamic flow with COMSOL multiphysics*. in *Proc. ESA Annual Meeting on Electrostatics, Paper E*. 2008.

34. Ghazanchaei, M., K. Adamiak, and G.P. Castle, *Predicted flow characteristics of a wire-nonparallel plate type electrohydrodynamic gas pump using the Finite Element Method.* Journal of Electrostatics, 2015. **73**: p. 103-111.

35. Ramadhan, A., N. Kapur, J. Summers, and H. Thompson, *Numerical modelling of electrohydrodynamic airflow induced in a wire-to-grid channel.* Journal of Electrostatics, 2017. **87**: p. 123-139.

36. Ramadhan, A.A., N. Kapur, J.L. Summers, and H.M. Thompson, *Numerical Analysis and Optimization of Miniature Electrohydrodynamic Air Blowers.* IEEE TRANSACTIONS ON PLASMA SCIENCE, 2017. **45**(11): p. 3007.

37. Karpov, S. and I. Krichtafovitch. *Electrohydrodynamic flow modeling using FEMLAB*. in *Excerpt from the Proceedings of the COMSOL Multiphysics User's Conference 2005 Boston*. 2005.

38. Feng, J.Q., *Application of Galerkin finite-element method with Newton iterations in computing steady-state solutions of unipolar charge currents in corona devices.* Journal of Computational Physics, 1999. **151**(2): p. 969-989.

39. Kaptsov, N., *Elektricheskie yavleniya v gazakh i vakuume.* Moscow, OGIZ, 1947.

40. Peek, F.W., *Dielectric phenomena in high voltage engineering*. 1920: McGraw-Hill Book Company, Incorporated.

41. Yen, S.-C. and J.-H. Liu, *PIV measurements of exit flow field of centrifugal fans with conditional sampling.* Journal of Marine Science and Technology, 2007. **15**(3): p. 232-240.

42. Abdel-Salam, M., M. Nakano, and A. Mizuno, *Corona-induced pressures, potentials, fields and currents in electrostatic precipitator configurations.* Journal of Physics D: Applied Physics, 2007. **40**(7): p. 1919.

43. Sunonwealth Electric Machine Industry Company Limited; Available from: http://www.sunon.com/index2/pro2.php?c1=10&c2=2.